Real time image processing based on-line feedback control system for cooling batch crystallization

Ákos Borsos[1], Botond Szilágyi[2], Paul Șerban Agachi [2,3], Zoltán K. Nagy[1,4]

[1]Department of Chemical Engineering, Loughborough University, Loughborough, LE11 3TU, United Kingdom

[2]Department of Chemical Engineering, Babeș-Bolyai University, Arany János Street 11, Cluj Napoca, Romania

[3] College of Engineering and Technology, Botswana International University of Science and Technology (BIUST), P. Bag 16, Palapye, Botswana

[4]School of Chemical Engineering, Purdue University, West Lafayette, IN, USA

Highlights

- Real time image processing based DNC system is developed and presented
- Converged, stable control of batch cooling crystallization was achieved in most cases
- The IA-DNC presents several advantages compared to the FBRM based DNC

---

*Corresponding author: School of Chemical Engineering, Purdue University, West Lafayette, IN, USA. Tel.: +1 7654940734, e-mail: zknagy@purdue.edu, z.k.nagy@lboro.ac.uk

TOC:

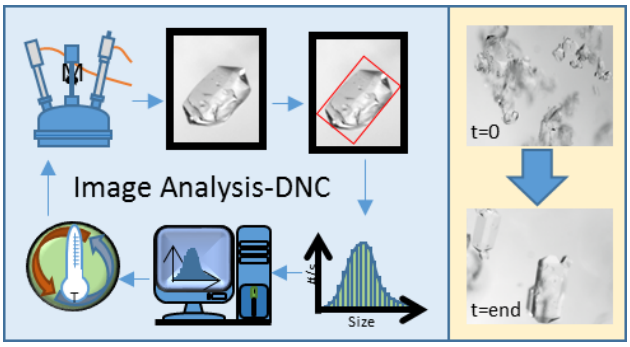

Abstract

The direct nucleation control (DNC) is a process analytical technique (PAT) based model free feedback control strategy for batch and continuous crystallization processes, which has been successfully applied in numerous cases. The basic principle of DNC is the use of controlled dissolution cycles to control a measurement directly related to the particle number in the system. During the DNC, in the case of cooling crystallization fines are dissolved by repeated heating-cooling loops. In this context, the controlled variable is the (relative) particle number, which is manipulated using a feedback control approach through the temperature. The particle number is traditionally measured with focused beam reflectance measurement (FBRM), however other PAT tools can also be employed in a similar feedback control setup. Often crystallization processes are also monitored by real-time imaging systems. In the current work a novel DNC setup is proposed in which microscopy images are captured and processed by the means of image analysis in real time. The images are used to extract the relative particle number, which is controlled using the DNC framework. The robustness of the new *image analysis based direct nucleation control* (IA-DNC) is presented via three case studies with materials having different crystallization properties. The IA-DNC approach uses a Particle Vision probe although other in situ or in line imaging systems can also be used in the framework. The systems are monitored with FBRM for comparison purposes. The setup achieved stable, converged control in most cases and is demonstrated that the IA-DNC has several advantages over the classical FBRM based DNC. The IA-DNC can also be used for real time feedback control of crystal shape.

Keywords: crystallization, image processing, direct nucleation control, process analytical technologies, model free control

1. Introduction

Crystallization is a key unit operation, a separation and purification technique in various chemical, pharmaceutical and food industries. The key descriptors of the crystalline materials are the size, shape, purity and polymorphic form. All these properties impact significantly the efficiency of downstream operations such as drying or filtration and influence product quality[1-3]. The Food and Drug Administration (FDA) and the European Medicines Agency (EMA) encourage the pharmaceutical and food companies to use Quality by Design (QbD) approaches for the sake of minimizing the variability in product properties[4].

Process analytical technology (PAT) brings numerous new methods and opportunities in the real-time monitoring of crystallization processes. These can be integrated into the control strategy and provide exhaustive information about the crystallization, opening new doors in deeper understanding of the fundamental governing processes also enabling the efficient design of crystallization systems by the application of feedback control strategies, according the a novel Quality-by-Control (QbC) framework[5]. The crystal size and shape distribution can be tracked by numerous methods. FBRM is an in situ measurement tool, which provides information about nucleation, growth, dissolution, polymorphic transformation, and size distribution of crystal population[4], however multiple crystal properties or operating conditions (e.g. mixing) can influence the measured signal. To obtain more robust measurement and identification of mechanisms during crystallization the combination of PAT tools is commonly implied. Saleemi et al. combined FBRM with attenuated total reflection ultraviolet/visible spectroscopy (ATR-UV/VIS) in order to detect the crystallization of isomers[6]. Simon et al. applied the same combination, supplemented with bulk video imaging (BVI)[7] while Liu et al. used FBRM, particle video microscopy and near-infrared spectroscopy (NIR)[8]. Polymorphic transformations were also investigated with combined PAT tools[9].

Limited number of research papers deal with FBRM based crystallization control. Kougoulos et al. applied FBRM and process video imaging in a modified mixed suspension

mixed product removal crystallizer to control the crystal size distribution (CSD)[10]. Aamir et al. proposed a control strategy of CSD by optimal supersaturation and seed recipe[11]. Sheikhzadeh et al. proposed a PAT based control for an anti-solvent crystallization[12]. Nagy developed a model based feedback control approach for batch crystallization, which is based on particle number detection[1]. Fujiwara et al. introduced first-principles and direct design approaches involving the FBRM count and concentration measurements[13]. Automated direct nucleation control (ADNC) was developed for crystal size control for batch processes by Salemi et al. and Abu Bakar et al.[14-16]. The concept was further extended to continuous processes and then combined with milling in order to generate larger number of particles[45,46].

In the recent years, image recording and processing tools have also been developed and widely applied for crystallization processes. These techniques are suitable for crystal shape monitoring and control[17]. An early work of image analysis based process monitoring and optical imaging was developed by Patience et al.[18] Today numerous companies provide in situ imaging sensors as well as flow-through cell imaging devices[2,5,19-20]. Endoscope based systems were also integrated into the process monitoring setup[7].

The vast majority of applications use imaging systems as a qualitative tool to monitor crystallization, with limited applications of real time quantitative application based on image analysis. The image analysis techniques used can be classified in two broad classes: (i) the blob analysis is based on particle boundary detection and (ii) the texture analysis monitors the change of image descriptors[5]. These tools have been successfully applied for nucleation detection[21-22], particle size[23] and shape monitoring[17,23-25] and monitoring polymorphic transformations[19-20,26-27]. Imaging techniques combined with additional PAT tools are also often used for monitoring e.g. morphological changes in various crystallization processes in the presence of additives[28,29,30]. Image analysis has also been applied for modeling purposes[2]. Ma and Wang applied closed loop crystal shape control, with morphological population balance model

validated based on post-processed in-line crystal images[31-32]. Borsos et al., used the ParticleView with particle vision and measurement (PVM) technology, for real time monitoring and open loop crystal aspect ratio (AR) control. Indeed, image processing techniques are spreading quickly, however the quantitative use of PVM for real time feedback control has not been reported yet[17].

In the current work an image analysis based direct nucleation control (IA-DNC) is proposed, which is tested in three case-studies for crystal size control. During the IA-DNC the system is also monitored with FBRM for comparison. It is shown that IA-DNC can successfully control crystal size distribution providing an alternative approach to the FBRM-based DNC, enabling the more direct control of particle numbers or other, for example shape related, crystal properties.

2. Image analysis based automated direct nucleation control IA – DNC

DNC is a model-free control approach, which uses data related to the particle number such as FBRM measured chord length distribution. Hence, a number related total count in a unit time is monitored and setpoint for the count can be provided. Based on the measured counts the temperature is manipulated in order to control the supersaturation, which determines the nucleation and growth rates. Higher supersaturation, generally, favors nucleation. Thus, the faster cooling leads to larger particle number and, consequently, to lower mean size. During heat-up crystal dissolution occurs. According to the Oswald ripening effect the dissolution rate is inversely proportional with the crystal size[38,39]. Ideally, the heating stage leads to dissolution of fines (fines is generally considered as small crystals in the 10s μm range), while moderately reducing the size of larger crystals. Consequently, cyclic temperature profile can lead to crystal population with narrower size distribution and larger mean size. This correlation between temperature cycling and CSD is used in the DNC approach for CSD control.

In the present work the PVM is applied as in-line imaging PAT tool. The captured images are post-processed in real time by using Blob image analysis method for detection of particles including segmentation, object (or edge) detection[5,40], as shown in Fig. 1, extracting the particle size, shape (AR) and relative particle number (counts/s). This example presents the numerically calculated grey frames around the detected particles. The frame edge lengths give information about the size and AR of the particle projection. The particle count obtained from the IA is, similarly to the FBRM measurement, directly proportional to crystal number: larger number of particles leads increased number of detections. It's limitation is the high solid concentration that can cause crystal overlapping, which translates to reduced chance of capturing individual crystals[41,42,43]. Increase in particle counts may be the result of formation of small particles (or nuclei) while the decrease can come from dissolution. When FBRM is used for monitoringthe crystallization of high AR crystals, the FBRM count will show increase in the numbers of fine chord lengths due to the higher probability of capturing the width of the crystals rather than the length. This artifact will be interpreted as nucleation event and the FBRM based DNC would trigger dissolution, leading to decrease of size. In these cases, the FBRM based DNC often leads to constant cycling and long batches without eventually converging to the final desired temperature. The key advantage of the IA-DNC is that the particle number measurement is completely decoupled from the shape of the crystals and is a true reflection of crystal nucleation or dissolution.

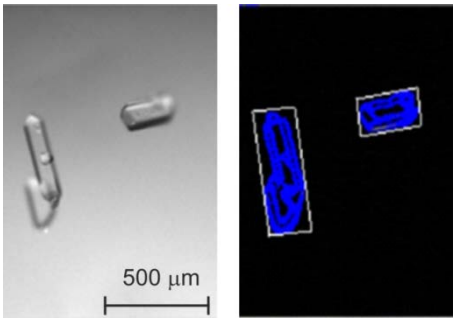

Figure 1. Real time PVM imaging and image processing

Fig.2 presents the flow diagram of the proposed IA-DNC. In situ measurements are accomplished by using PVM. The captured images (10fps) are post-processed in real time by the Lasentec Particle Vision Microscope Image Acquisition V8.3.0.55 software (Mettler Toledo, USA), calculating the crystal size and shape distribution as well as the relative particle number. Settings for image processing was tuned in preliminary experiments in order to obtain the best results in terms of object detection. The parameters were: threshold limits (8-231), decimal factor (5), edge filter (Sobel) and minimum pixel size (20). The extracted crystal properties are transmitted to the crystallization process informatics system (CryPRINS) software, which is an in-house developed software platform for crystallization monitoring and control. CryPRINS is a software used to monitor and control crystallization processes by automatically collecting and handling data from a variety of PAT tools (http://www.cryprins.com). Automatic control approaches such as supersaturation control (SSC) or DNC are implemented in CryPRINS which manipulates the temperature to control the concentration or crystal counts, while respecting the user-provided parameters and constraints .

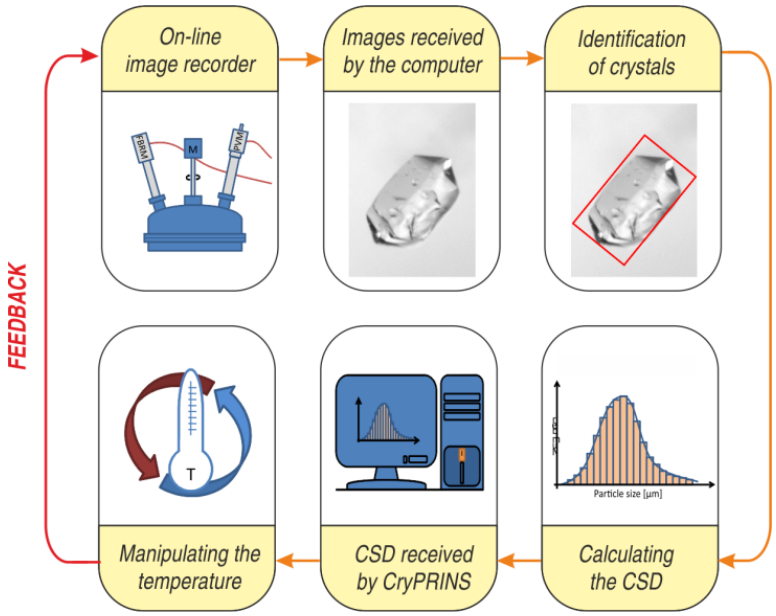

Figure 2. Working principle of the proposed IA–DNC approach.

The IA-DNC system with the experimental setup is presented in Fig. 3. PVM (Mettler Toledo, PVM V819) sensor is used as the imaging tool for feedback control, which provides crystal size and shape distribution as well as the (PVM) count; FBRM (Mettler Toledo, Lasentec FBRM D600VL) is applied for process monitoring of chord length distribution (CLD) (a "fingerprint" of particle population) and (FBRM) counts; ATR-UV/VIS spectroscopy for concentration measurement, when possible. The CryPRINS collects the data from all probes and manipulates the crystallizater temperature by controlling the thermostat (Huber Ministat cc3).

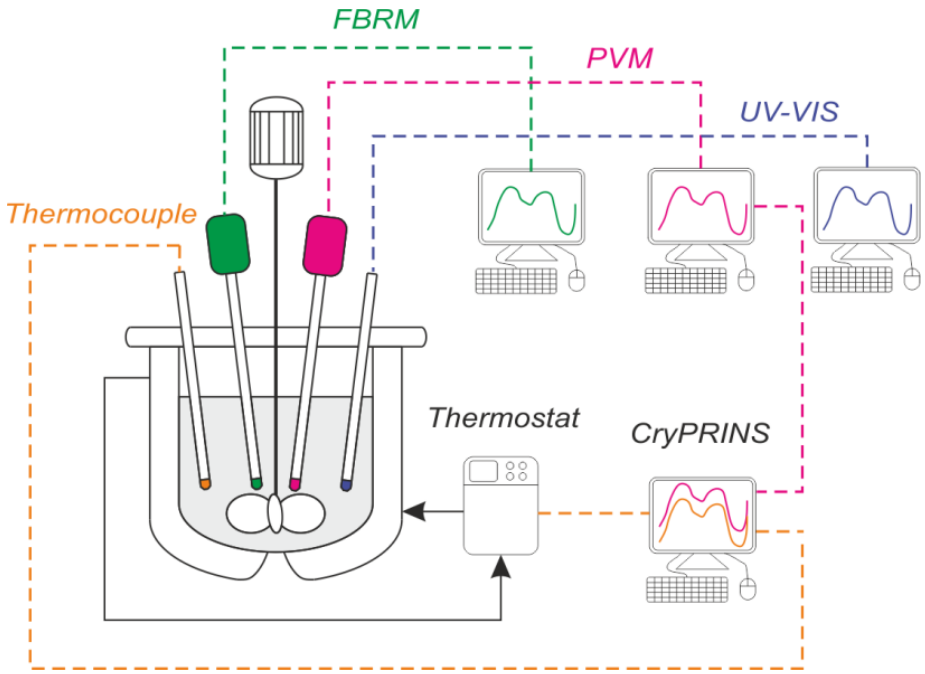

Figure 3. Schematic representation of the experimental setup with the PAT tools used

3. Results and discussion

Table 1 presents the composition of applied chemical systems. Crystallization of potassium di-hydrogen phosphate (KDP) from water was used as model system in two forms: in aqueous solution (Exp. 1) and aqueous solution in presence of impurities (Exp. 2). The trace amount of

impurity leads to significantly different crystallization kinetics. This enabled to investigate the effect of different crystal AR and kinetics on the IA-DNC performance, while maintaining other crystallization conditions similar. The third case study used a different compound, an active pharmaceutical ingredient, L-ascorbic acid in water (Exp.3). These three systems represent considerably different crystallization behaviors providing a suitable experimental set to analyze the performance of the IA-DNC.

Table 1. Composition of solutions applied in case studies and the used PAT tools

	Chemical compounds		**Tracked properties**			
Exp.	**Solute mass [g]**	**Solvent mass [g]**	**FBRM CLD**	**PVM CSD**	**PVM AR**	**UV-Vis**
1 – KDP	94	250	+	-	+	-
2 – KDP	94	250	+	+	-	-
3 – L-AA	100	250	+	-	+	+

The "+" denotes which properties were measured in the experiments, while properties marked with "-" was not monitored during the process.

3.1 KDP crystallization from aqueous solution

The KDP crystallization has well-known crystallization kinetics[17,33-34]. Two IA-DNC experiments were carried out applying different cooling and heating rates (0.3 ^{o}C/min and 0.5 ^{o}C/min) in order to handle the PVM based count number at a certain value (it is 2.7 in the "slow" and 3.9 in the "fast" cooling experiments). The systems in both cases were cooled down to 20 ^{o}C. Palliation of the heating and cooling rates can be done between the limits of counts by using the gain factor. This reduces the heating rate when the count number achieves the setpoint (desired count number) and keeps the temperature on the reduced rate until it reaches the pre-

defined lower limit of the count number. It also reduces the cooling rate between the setpoint and upper limit of counts ($\Delta T_{mod} = \Delta T / Gain\ factor\ \ when\ No._{min} < \# < No._{max}$). This is for reducing the amplitude of the count and improving the efficiency of the temperature control. The same gain factor of 2 for the heating and cooling rates were applied in the experiments.

Fig.4a presents the results of "fast" IA-DNC working with the more intensive, 0.5 ^{o}C/min heating and cooling rate in which experiment the process ended up in 205 minutes. After 3 temperature cycles the desired final temperature (T_{final} = 20C) is achieved and stabilized while the setpoint was kept between the upper and lower count limits. The FBRM and PVM counts show similar trends (green dotted and blue solid lines), with three order of magnitude difference in absolute values, which is resulted from the different particle capturing technique behind the two sensors. This is due to the fact that less crystals could be captured by the imaging probes such as PVM (see Fig.5) in a unit time (10fps and 30sec sample time were applied). This also explains the larger noise in the PVM count than in the FBRM signal. This can be improved by using larger sampling time, which means more images would be analyzed for one measurement. The comparison shows that imaging technique, and the particle count from image analysis, could be used for robust control of crystallization systems but uncertainty and noise are larger than using FBRM.

Fig.4b presents the time evolution of mean particle properties during the crystallization. The mean square weighted chord length from the FBRM indicates that the particles are growing with each IA-DNC cycle. In these experiments the PVM recorded the "mean AR", the ratio of two characteristic crystal sizes, which naturally provides shape/morphology related information. It can be observed that the AR increased during the heating and slightly decreased during the cooling stages. This can be caused by the different growth and dissolution rates of the faces of KDP under the investigates conditions. This might also be related to nucleation and to fines dissolution as the AR of fines is generally recognized close to 1.

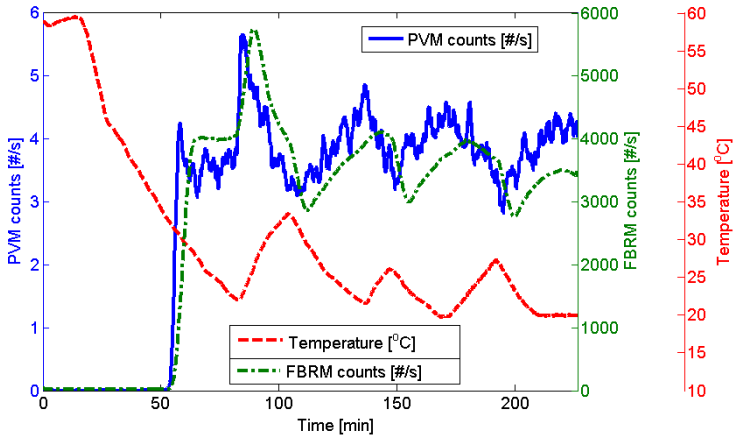
PVM counts [#/s]
Temperature [°C]
FBRM counts [#/s]
PVM counts [#/s]
FBRM counts [#/s]
Temperature [°C]
Time [min]

a)

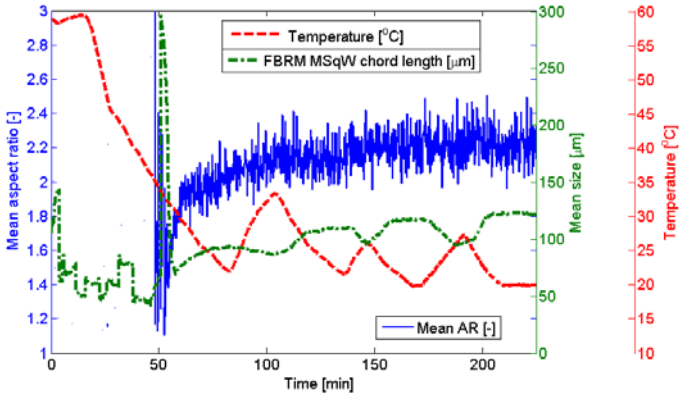
Temperature [°C]
FBRM MSqW chord length [μm]
Mean AR [-]
Mean aspect ratio [-]
Mean size [μm]
Temperature [°C]
Time [min]

b)

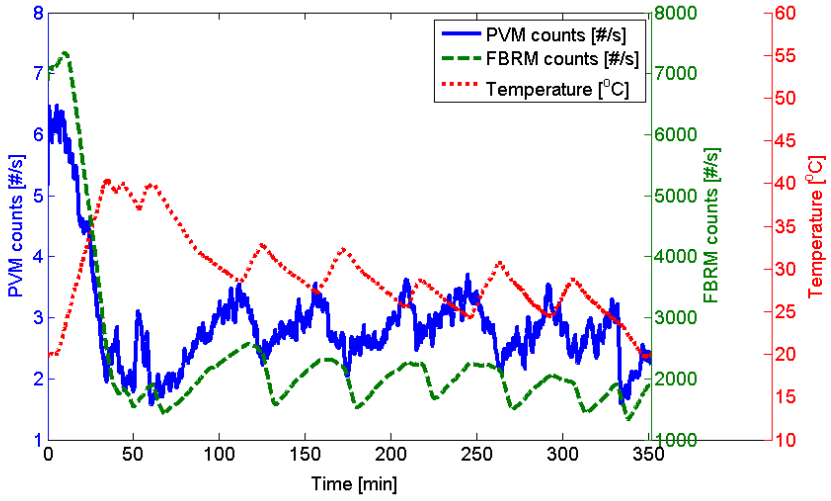
PVM counts [#/s]
FBRM counts [#/s]
Temperature [°C]
PVM counts [#/s]
FBRM counts [#/s]
Temperature [°C]
Time [min]

c)

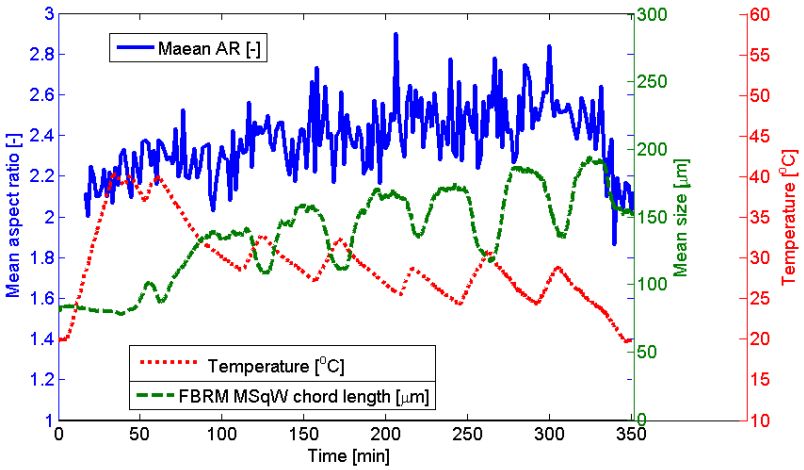

d)

Figure 4. IA-DNC of KDP a) FBRM and PVM counts and temperature and b) evolution of mean chord length and mean AR during the "Fast" crystallization; c) FBRM and PVM counts and temperature and d) trends of mean particle chord length and mean AR during the "Slow" crystallization.

Figure 4a and fig. 4b show the measured trends of crystallization during "slow" IA-DNC. It is also a stable control, when the desired count and the temperature were achieved after 5 DNC cycles and it resulted higher AR (close to 2.6) of the product crystals. The lower value for setpoint led to significant increase of the measurement noise and the trend of mean AR is more intensive. The FBRM count number is also halved compared to the "fast" DNC, and the measurement is still robust in terms of accuracy.

Fig.5 presents the PVM images of products obtained at the end of the "fast" and "slow" DNC experiments. It is evident that the "slow" IA-DNC produced less agglomerated crystals but it also took 60% more time (350 min vs. 220 min). This can be explained by the fact that the fast cooling generated high supersaturation, which finally leads to more and stronger agglomerates, which are more resistant to dissolution and are not destroyed in the heating stage. According to the figures 4 and 5, the AR (the agglomerates are handled as a single particle by

the image processing software) obtained from the slower IA-DNC is in fact higher than in the fast DNC where agglomearates were produced.. This indicates that in fact the larger number of cycles in the slow IA-DNC experiments, as expected, help to obtain less agglomerate product, while the process conditions led to slightly higher AR. This also indicates that the IA based DNC could also be used in real-time shape control.

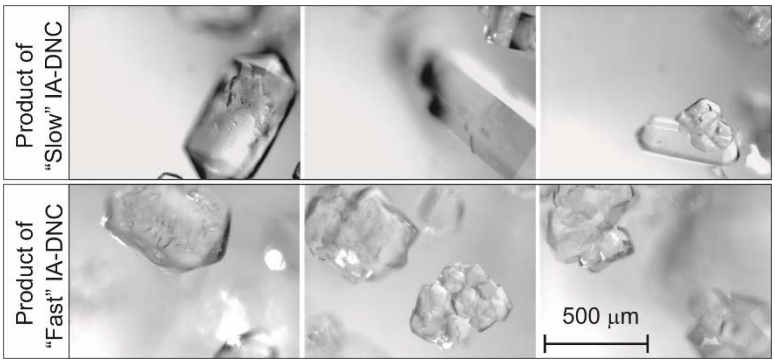

Figure 5. PVM images of KDP crystal product obtained from "Slow" and "Fast" IA-DNC experiments.

Sticking of crystals on the probes often occurs during the nucleation, as the PVM image sequence of Fig. 6 illustrates. This worsens the measurement accuracy (for FBRM and PVM too), however image processing provides good opportunity to digitally hide the pixels where particles arestuck.

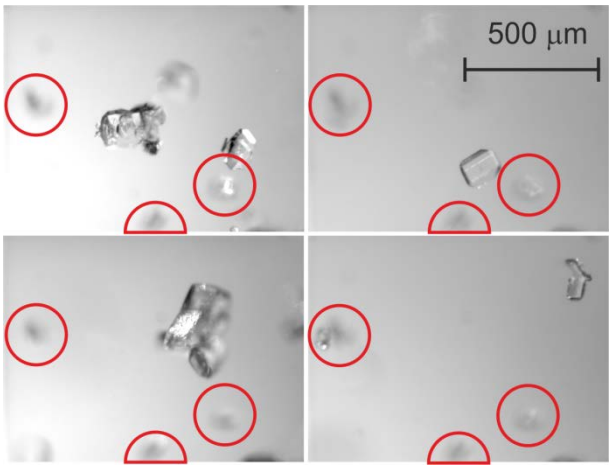

Figure 6. PVM image sequences during nucleation and growth with sticking particles on the PVM sensor.

3.2 KDP crystallization from aqueous solution in the presence of impurity

A fresh solution of KDP was prepared by dissolving 94 g substance in 250 g distilled water, which corresponds to the solubility at 40 ^{o}C. As it was investigated in recent studies, the KDP, in the presence of impurities, shows quite different crystallization kinetics. Borsos et al., (2016) studied the effect of multi-impurity adsorption on the crystal shape and purity[44]. The paper explains the strong effect on the AR of crystals and the same effect is now considered to be investigated when sequential cooling-heating cycles are used. Low quantity of impurity (Aluminum sulphate) was added to the solution in ppm concentration domain.

The experiment is carried out with 0.15 ^{o}C/min cooling and 0.2 ^{o}C/min heating rates and high gain factors (3 for cooling and 2 for heating) were used during the process. This parameterization leads to a very slow DNC. The final temperature is as in the case of pure KDP crystallization, 20C. CryPRINS was also used to collect data and control the crystallization via temperature profile. Setpoint for the PVM counts was set to 11 #/sec, while the settings of image analysis in the PVM image acquisition software are the same as in the previous section.

Fig. 7a presents the time evolution of FBRM and PVM counts during the batch, which exhibit similar trends. There are however some noticeable differences: when the system switches to heating the FBRM count increases (indicating the disintegration of agglomerates), which tendency is not presented in the PVM count. The FBRM count behaves as an inverse response system, for which the control might become challenging. Optionally ignoring the smaller particles from the FBRM CLD may be solution for the inverse response problem. However, filtering small particles from the measured CLD might inherently leads to delay in

the detection of nucleation and raises additional issues on *how* the CLD should be (optimally) reduced.. When the particle sizes in the agglomerates are below the limit of the detectable size of the object, the PVM does not detect these fines, which act as a filter. The limitation of the detection can be either physical such as the resolution of the imaging sensor, the limited availability of the optical imaging in under 10 µm or software based limitation originated the values of the analyzer such as threshold and other parameters[40-43]

Finally, it can be seen that the IA-DNC kept the PVM counts between the predefined limits (Fig.7a) and stable, converged control is still achieved.

The FBRM mean square weighted chord length continuously increases with the number of DNC cycles but the PVM mean diameter slightly decreases (Fig.7b). This may be because the biggest crystals grew out of the PVM range. Additionally, the solid density in the system may be close to the limitation of the image processing and large crystal are not accurately captured. with the applied image processing setup. Fig.7c presents the PVM images at the end of the cooling stages, highlighting that the agglomerates gradually disappear and the crystals exhibit significant growth.

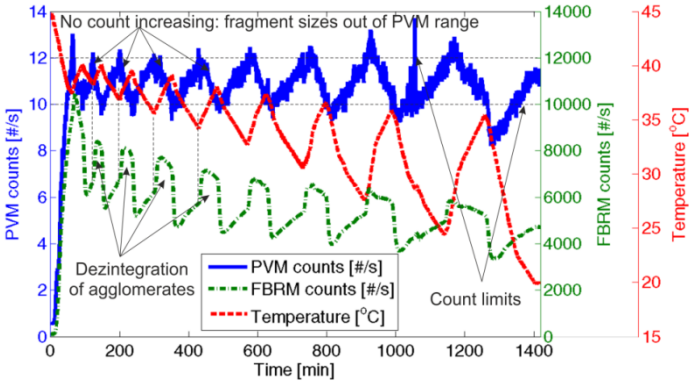

a)

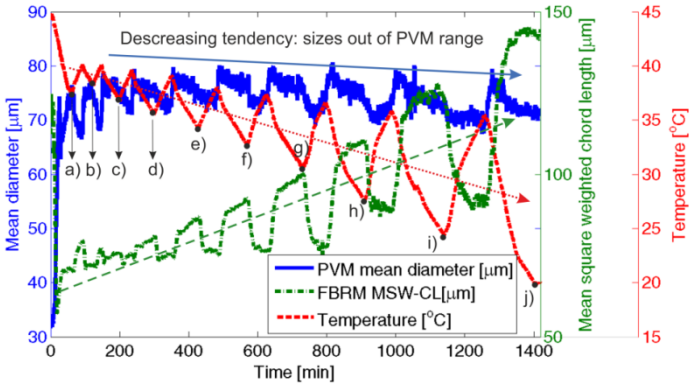

b)

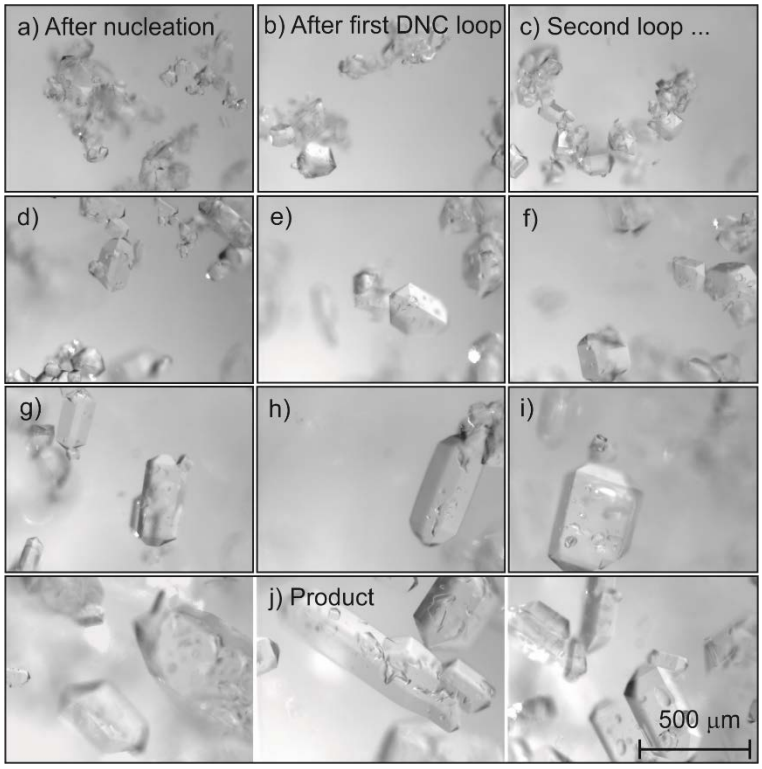

c)

Figure 7. IA-DNC of KDP crystallization in presence of impurities a) FBRM and PVM counts b) particle sizes provided by FBRM and PVM and c) PVM images of crystals in time moments indicated in Fig.7b

Figure 8 presents the temporal evolution of the chord length distribution measured by the FBRM. Fig 8a shows that the nucleation generates high count, and a relative narrow CLD at the beginning. According to the figure the chord lengths are growing from cycle to cycle but

the CLD becomes wider. The color map of the figure surface (Fig. 8b) indicates that the crystals are not completely dissolved, the CLD just moves to the lower chord length range during the heat-up stages as it was expected during the sequential cooling-heating temperature profile.

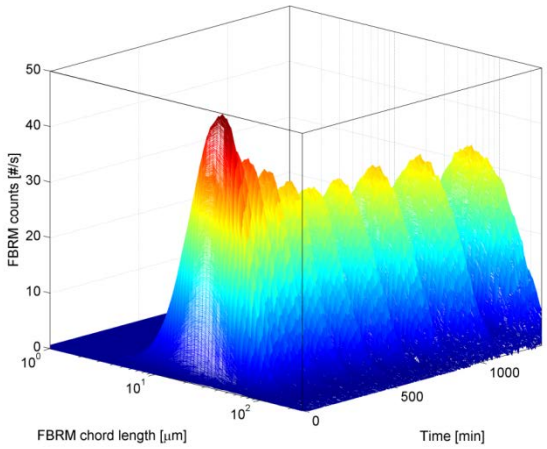

a)

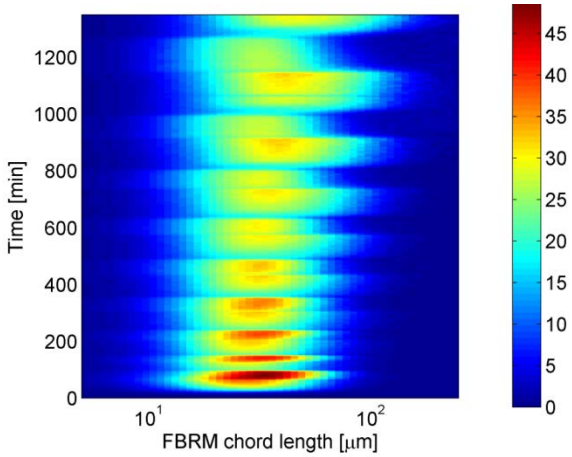

b)

Figure 8. a) Time evolution of CLD during the IA-DNC and b) Color map of Fig. 8a (Color bar: #/s).

According to these results, the IA-DNC is suitable to control the crystallization of materials having increased agglomeration inclination. Comparing the count provided by the FBRM and PVM it was observable that PVM with given IA settings (which is common to use to avoid

noise in the images) does not detect the particle sizes coming from the agglomerate disintegration. In this situation the FBRM count behaved as an inversed response system, which is not advantageous in process control and would lead to larger number of oscillation. However, limitation of the IA-DNC is that during the crystallization the particles can grow out from the PVM detection limit.

3.3 L-ascorbic acid crystallization from water

Eggers et al. monitored the shape and size during the seeded cooling batch crystallization of L-ascorbic acid[23]. Other studies investigated the crystallization kinetics from ethanol-methanol-water system reporting interesting correlations between the fundamental phenomenon of solubility, nucleation, growth and the system properties with solvent composition and temperature[35-37]. However, none of these studies considered the control of L-ascorbic acid crystallization.

Aqueous solution of L-ascorbic acid was prepared by dissolving 100 g acid in 250 g solvent, resulting saturated concentration at 40 ^{o}C in the solution. In the case of L-ascorbic acid crystallization, 0.2 ^{o}C/min cooling and heating rates with gain factor of 2 (for both) were applied. The lower temperature limit was set to 15 ^{o}C. Seeds were added to the supersaturated solution, because primary nucleation did not occur in the used temperature range. Seeds help reducing supersaturation in the first cycling loop.

Fig. 9a presents the evolution of PVM and FBRM counts during the IA-DNC run. Both sensors indicate similar trends. The IA-DNC kept the number of particles between the predefined limits, which, however, presented sustained oscillations. These oscillations are related to the crystallization kinetics; for this system the growth is relatively slow and the secondary nucleation becomes intensive at higher supersaturation. As shown on Fig. 9a, after the longer cooling cycles during the first part of the batch, the FBRM counts increases but the

PVM count does not. The delay in the PVM to detect nucleation events introduces considerable dead time in the closed-loop feedback control system, based on the PVM measurement, which is set to detect larger particle sizes. The controllability of systems high with large dead time is generally more difficult and feedback control can easily lead to oscillations. Generally, two options exist to improve controllability: (i) slowing down the process to reduce the time constant/dead time ratio i.e. by applying slower heating/cooling rates (this is however un-favored since can lead to excessive batch time) or (ii) the application of some predictive technique. Because to the advantageous properties of on-line imaging to give size and shape information, this technique might have a prominent role in a model based control strategy as measuring tool. An interesting observation is that, according to Fig. 9b, the mean AR is sensitive to the DNC cycles. Theoretically the growth and dissolution rates of different faces may differ and may lead to shape variationswhen supersaturation (driven by, for instance, temperature change, or using anti solvent, etc.) changes during crystallization. This can be more intensive when growth/dissolution is size dependent[20,44]. Hence, the shape of the nuclei and the grown crystals are different (nuclei is closer to the spherical shape) and thus AR decreases with the nucleation and can increase with the fines dissolution. This is in good agreement with the observations of KDP crystallization, suggesting, again, the possibility of using the image analysis based DNC for shape control.

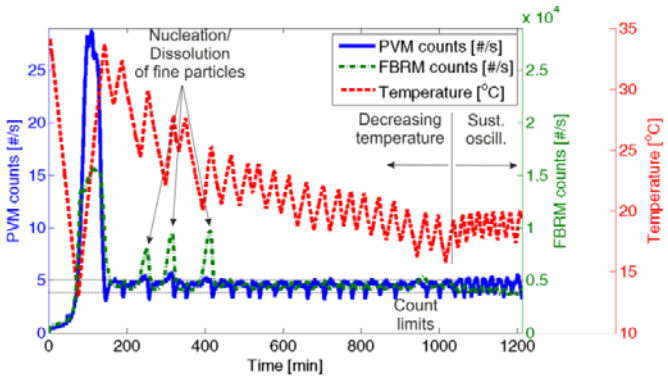

a)

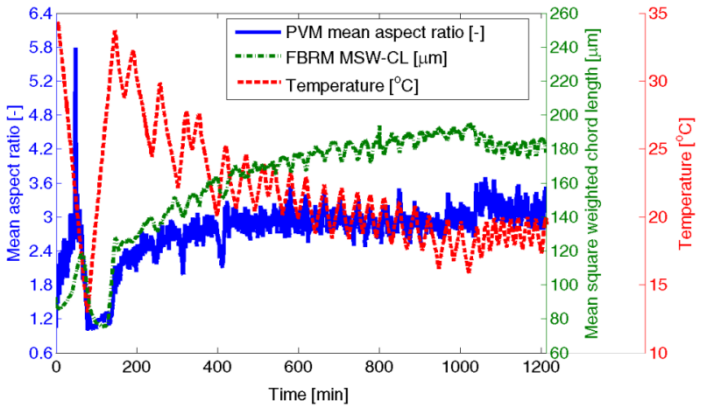

b)

Figure 9. IA-DNC of L-ascorbic acid batch crystallization: a) PVM and FBRM counts and **b)** Shape and size variations during the batch.

Fig. 10 presents the phase diagram of the first part of the IA-DNC (the later loops are not represented to avoid the figure overloading). In the first cycle the solution is cooled almost to the lowest temperature, despite of the seed addition. The intensive cooling generates high crystal number, which is dissolved by an intensive heating stage. This plot highlights well the large time delay characteristic for this process. This intensive cooling and heating can be avoided if larger amount of seed is added or slower cooling is applied. However, the presented experiments are good examples of the robustness of the DNC concept.

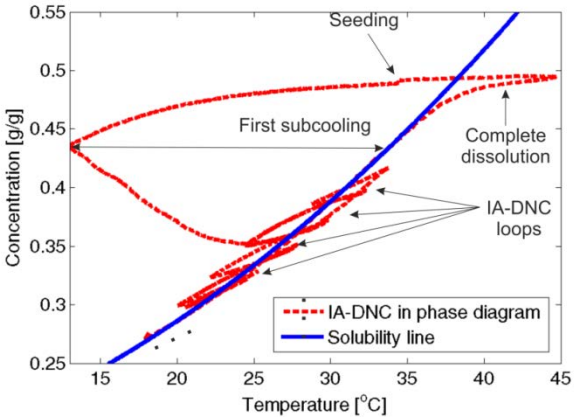

Figure 10. IA-DNC operating curve in the crystallization phase diagram. The first nucleation loop if followed by smaller, oscillating cycles.

Fig. 11 illustrates the PVM images in different stages of the batch: the newly formed crystals, an intermediate stage at the end of heating and a representative snapshot from the sustained oscillation zone. According to the figures, the AR of the small crystals is close to 1, while the bigger crystals have plate-like habit with higher AR. As the PVM captures two dimensional projections of the crystals, the plate like shape generates increased AR in the image processing procedure.

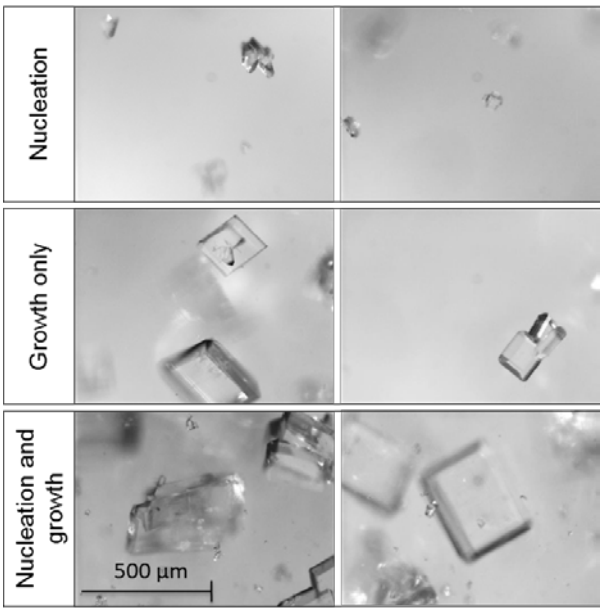

Figure 11. PVM images a) during the first nucleation process, b) after dissolution and c) during the multiple cooling stages of L-ascorbic acid crystallization.

In the case of the L-ascorbic acid crystallization the IA-DNC does not perfectly converges to the final desired temperature. However, the temperature oscillates in a relatively narrow domain and, according to the Fig. 11, high quality, large product crystals are obtained. The fines could simply be removed by a final dissolution overall making the IA-DNC an efficient approach for the crystallization of L-ascorbic acid.

According to the results, in some situations the IA-DNC is more attractive but for other systems/materials the FBRM based DNC remains the better choice. Hybrid control strategies could simultaneously benefit from the advantages of PVM and FBRM. An intelligent decision system could be developed, which could decide whether if the PVM or FBRM signal is the more representative. As a simple example, the FBRM based DNC often may not suitable for the control of the crystallization of growth dominated high AR crystals. In these cases, due to the increased growth in the length direction, the probability of measuring chord lengths determined by the width of the particles increases, and if the system is growth dominated the increase in the total counts/s predominantly will be due to the growth in the length direction. This increase in total counts will be interpreted by the DNC algorithm as nucleation event and dissolution cycles will be initiated, which then will decrease the length of particles, thus decreasing the total counts. This generally leads to sustained oscillations if DNC is implemented based on the FBRM counts. Since IA approaches identify the number of particles independently of their shape the increase in number of counts resulting from the images is always the result of true nucleation, hence the IA-DNC can be a more suitable approach for these systems. Another example for the potential benefits of combined use of the FBRM and PVM based DNC can be to use at the beginning of the crystallization when solid concentration maybe lower the IA-DNC, since IA based techniques give a better estimate of particle count, but as solid concentration increases, due to overlapping particles the PVM images can saturate in later stage of the crystallization when the DNC could switch to using signal from the FBRM that is sensitive to changes in particle number even in relative high solid concentrations. The switch could be done by an automated decision support system, by comparing the trends of the PVM and FBRM counts.

4. Conclusions

In the current work an extension of the direct nucleation control (DNC) is presented, where on-line imaging based real time image processing provides the particle properties for the feedback controller. PVM is used for on-line imaging and FBRM for process monitoring. Based on the presented three case studies the real time image analysis can be successfully adopted into the DNC approach. The agreement between the FBRM and PVM provided count trends was acceptable.

The study demonstrated that the PVM count has several advantageous properties: (i) artefact in signal due to sticking could easily be corrected digitally in the image processing; (ii) the inverse response of FBRM count at the heating stage (due to the disintegration of agglomerates) not appears in the PVM count; (iii) the image processing based count is generally more reliable in the case of high AR crystals and (iv) the shape information, also provided by the PVM, can make the IA-DNC suitable for model free feedback control of shape.

According to the experiments, the crucial point of control system efficiency is the image processing setup as the used blob analysis based particle identification, generally, was reliable in limited size range. In order to enhance the control performance, the PVM based IA-DNC presented in the case-studies involved carefully tuned image processing to the expected particle size range of batch.

Some hybrid techniques are also suggested but in order to clarify the applicability and performance of those approaches further investigations are required.

Acknowledgements

Funding is acknowledged from the European Research Council under the European Union's Seventh Framework Program (FP7/2007-2013)/ERC grant agreement No. [280106-CrySys]. This work was possible due to the financial support of the Sectorial Operational Program for

Human Resources Development 2007-2013, co-financed by the European Social Fund, under the project number POSDRU/159/1.5/S/132400 with the title „Young successful researchers – professional development in an international and interdisciplinary environment".

References

(1) Nagy, Z.K. *Comp. Chem. Eng*. 2009, 33, 1685.

(2) Nagy, Z.K., Braatz, R.D. *Ann. Rev. Chem. Bimol. Eng*. 2012, 3, 55.

(3) Larsen, P.A., Rawlings, J.B., Ferrier, N.J. *Chem. Eng. Sci.* 2006, 61, 5236-5248.

(4) Saleemi, A.N., Rielly, C.D., Nagy, 2 Z.K. *CrystEngComm*. 2012, 14, 2196.

(5) Nagy, Z.K., Fevotte, G., Kramer, H., Simon, L.L. *Chem. Eng. Res. Des*. 2013, 91, 1903.

(6) Saleemi, A.N., Rielly, C.D., Nagy, Z.K. *Chem. Eng. Sci*. 2012, 77, 122.

(7) Simon, L.L., Nagy, Z.K., Hungerbuhler, K. *Chem. Eng. Sci*. 2009, 64, 3344-3351.

(8) Liu, X., Sun, D., Wang, F., Wu, Y., Chen, Y., Wang, L. *J. Pharm. Sci*. 2011, 100, 2452.

(9) Simone, E., Saleemi, A.N., Nagy, Z.K. *Chem. Eng. Res. Des*. 2014, 92, 594.

(10) Kougoulos, E., Jones, A.G., Jennings, K.H., Wood-Kaczmar, M.W. *J. Cryst. Growth*. 2005, 273, 529.

(11) Aamir, E., Nagy, Z.K., Rielly, C.D. *Chem. Eng. Sci*. 2010, 65, 3602.

(12) Sheikhzadeh, M., Trifkovic, M., Rahoni, S. *Chem. Eng. Sci*. 2008, 63, 829.

(13) Fujiwara, M., Nagy, Z.K., Chew, J.W., Braatz, R.D. *J. Proc. Cont.* 2005, 15, 493.

(13) Saleemi, A.N., Steele, G., Pedge, N.I., Freeman, A., Nagy, Z.K. *Int. J. Pharm*. 2012, 430, 56.

(15) Saleemi, A.N., Rielly, C.D., Nagy, Z.K. *Cryst. Growth Des*. 2012, 12, 1792.

(15) Abu Bakar, M.R., Nagy, Z.K., Saleemi, A.L., Rielly, C.D. *Cryst. Growth Des*. 2009, 9, 1378.

(17) Borsos, A., Majumder, A., Nagy, Z.K. *Cryst. Growth Des*. 2016, 16, 555.

(18) Patience, D.B., Rawlings, J.B. *AIChE J*. 2001, 47, 2125.

(19) Wang, X.Z., De Anda, J.C., Roberts, K.J., Li, R.F., Thomson, G.B., White, G. *KONA Powder Part*. 2005, 23, 69.

(20) Lovette, M.A., Browning, A.R., Griffin, D.W., Sizemore, J.P., Snyder, R.C., Docherty, M.F. *Ind. Eng. Chem. Res*. 2008, 47, 9812.

(21) Simon, L.L., Oucherif, K.A., Nagy, Z.K., Hungerbuhler, K. *Ind. Eng. Chem. Res*. 2010, 49, 9932.

(22) Simon, L.L., Oucherif, A.O., Nagy, Z.K., Hungerbuhler, K. *Chem. Eng. Sci*. 2010, 65, 4983.

(23) Presles, B., Debayle, J., Rivoire, A., Pinoli, J-C., Fevotte, G. Proceedings in: *Conference of Societe Francaise de Genie des Procedes (SFGP)*, 2009, Marseille, France.

(24) Kempkes, M., Vetter, T., Mazzotti, M. *Chem. Eng. Res. Des*. 2010, 88, 447.

(25) Schorsch, S., Ochsenbein, D.R., Vetter, T., Morari, M., Mazzotti, M. *Chem. Eng. Sci*. 2014, 105, 155.

(26) Wang, X.Z., De Anda, J.C., Roberts, K.J. *Chem. Eng. Res. Des*. 2007, 8, 921.

(27) De Anda, J.C., Wang, X.Z., Roberts, K.J. *Chem. Eng. Sci.* 2005, 60, 1053.

(28) Simone, E., Cenzato, M.V., Nagy, Z.K. J. Cryst. Growth. 2016, 446, 50.

(29) Klapwijk, A.R., Simone, E., Nagy, Z.K., Wilson, C.C. *Cryst. Growth Des*. DOI: 10.1021/acs.cgd.6b00465

(30) Pataki, H., Csontos, I., Nagy, Zs.K., Vajna, B., Molnar, M., Katona, L., Marosi, Gy., *Org. Process Res. Des*. 2013, 17, 493.

(31) Ma, C.Y., Wang, X.Z. *Chem. Eng. Sci*. 2012a. 70, 22.

(32) Ma, C.Y., Wang, X.Z. *J. Proc. Cont*. 2012, 22, 72.

(33) Gunawan, R., Ma, D.L., Fujiwara, M., Braatz, R.D. *Int. J. Modern Phys*. 2002, 16, 367.

(34) Sun, C., Xue, D. Opt. Mat. DOI: 10.1016/j.optmat.2013.12.019

(35) Wierzbowska, B., Matynia, A., Piotrowski, K, Koralewska, J. *Chem. Eng. Proc*. 2007, 46, 351.

(36) Wierzbowska, B., Piotrowski, K., Koralewska, J., Matynia, A. *Chem. Biochem. Eng. Quart*. 2008, 22, 327.

(37) Wierzbowska, B., Piotrowski, K., Koralewska, J., Matynia, A. Polish J. Chem. Techn. 2008, 10, 60.

(38) Lifshitz, I.M., Slyozov, V.V. J. Phys. Chem. Solids, 1961, 19, 35.

(39) Simakin, A.G., Bindeman, I.N. J. Volc. Geotherm. Res. 2008, 177, 997.

(40) Sarkar, D., Doan, X-T., Ying, Z., Srinivasan, R. Chem. Eng. Sci. 2009, 64, 9.

(41) Larsen, P.A., Rawlings, J.B., Part. Part. Syst. Charact. 2008, 25, 420.

(42) Rawlings, J.B., Ni, X-W., CrystEngComm, 2012, 14, 2944.

(43) Simon, L.L., Merz, T., Dubis., S., Lieb, A., Hungerbuhler, K., Chem. Eng. Res. Des. 2012, 90, 1847.

(44) Borsos, A., Majumder. A., Nagy, Z.K. Cryst. Growth Des. 2016, 16, 555.

(45) Yang, Y., Song, L., Nagy, Z.K. Cryst. Growth Des., 2015, 15, 5839.

(46) Yang, Y., Song, L., Zhang, Y., Nagy, Z.K. Ind. Eng. Chem. Res. 2016, 55,4987.